



This is a repository copy of *Modelling the interactions between tumour cells and a blood vessel in a microenvironment within a vascular tumour*.

White Rose Research Online URL for this paper:  
<http://eprints.whiterose.ac.uk/1563/>

---

**Article:**

Breward, C.J.W., Byrne, H.M. and Lewis, C.E. (2001) Modelling the interactions between tumour cells and a blood vessel in a microenvironment within a vascular tumour. *European Journal of Applied Mathematics*, 12 (5). pp. 529-556. ISSN 0956-7925

<https://doi.org/10.1017/S095679250100448X>

---

**Reuse**

Unless indicated otherwise, fulltext items are protected by copyright with all rights reserved. The copyright exception in section 29 of the Copyright, Designs and Patents Act 1988 allows the making of a single copy solely for the purpose of non-commercial research or private study within the limits of fair dealing. The publisher or other rights-holder may allow further reproduction and re-use of this version - refer to the White Rose Research Online record for this item. Where records identify the publisher as the copyright holder, users can verify any specific terms of use on the publisher's website.

**Takedown**

If you consider content in White Rose Research Online to be in breach of UK law, please notify us by emailing [eprints@whiterose.ac.uk](mailto:eprints@whiterose.ac.uk) including the URL of the record and the reason for the withdrawal request.



[eprints@whiterose.ac.uk](mailto:eprints@whiterose.ac.uk)  
<https://eprints.whiterose.ac.uk/>

# Modelling the interactions between tumour cells and a blood vessel in a microenvironment within a vascular tumour

C. J. W. BREWARD<sup>1,2</sup>, H. M. BYRNE<sup>2</sup> and C. E. LEWIS<sup>1</sup>

<sup>1</sup>*Section of Oncology and Pathology, Division of Genomic Medicine,  
University of Sheffield Medical School, Beech Hill Road, Sheffield S10 2RX, UK*

<sup>2</sup>*School of Mathematical Sciences, University of Nottingham,  
University Park, Nottingham NG7 2RD, UK*

(Received 13 July 2000; revised 26 January 2001)

In this paper, we develop a mathematical model to describe interactions between tumour cells and a compliant blood vessel that supplies oxygen to the region. We assume that, in addition to proliferating, the tumour cells die through apoptosis and necrosis. We also assume that pressure differences within the tumour mass, caused by spatial variations in proliferation and degradation, cause cell motion. We couple the behaviour of the blood vessel into the model for the oxygen tension. The model equations track the evolution of the densities of live and dead cells, the oxygen tension within the tumour, the live and dead cell speeds, the pressure and the width of the blood vessel. We present explicit solutions to the model for certain parameter regimes, and then solve the model numerically for more general parameter regimes. We show how the resulting steady-state behaviour varies as the key model parameters are changed. Finally, we discuss the biological implications of our work.

## 1 Introduction

Tumour development occurs in two distinct stages. Initially, tumour cells in small avascular tumours gain the oxygen and nutrients they need for survival and growth by diffusion from the existing vasculature in the normal tissue that surrounds the tumour. The amount of oxygen thus supplied is limited by the surface area of the growing tumour while the amount of oxygen required by the cells is proportional to their total volume. In consequence, the tumour reaches a diffusion-limited size, where the amount of oxygen and nutrients entering balances the amount consumed by the live tumour cells (that exist near the rim of the tumour). The size of such a tumour is limited to 1–2 mm [16]. The cells near the centre of such tumours are subjected to hypoxic stress (that is, low oxygen tensions which gradually ‘suffocate’ the cells). Exposure to this stress slows their rate of proliferation and stimulates them to express diffusible factors such as Vascular Endothelial Growth Factor (VEGF), Tumour Necrosis Factor (TNF- $\alpha$ ), Transforming Growth Factor (TGF- $\beta$ ), which travel outwards from the tumour, towards the surrounding vasculature [6]. Once these factors reach the surrounding blood vessels, they stimulate endothelial cells lining the walls of the blood vessels to proliferate, migrate and differentiate to form new blood vessels which grow towards the tumour. Formation of new blood vessels by this

process is called tumour angiogenesis [6]. Once the vessels have reached the tumour and circulatory loops have formed, blood can flow through the vessels and supply the tumour cells with additional oxygen and nutrients. Vascular tumour growth then commences.

During vascular tumour growth, previously dormant cells that are close to the neovasculature are able to proliferate once again and the growth of the tumour as a whole can recommence. This may become life threatening for the host, since both the tumour and any metastases (secondary tumours that form when tumour cells escape from the primary tumour into the general blood or lymph circulation and establish colonies in other tissues) may cause malfunction of vital organs [10].

It is events associated with the vascular phase of tumour growth that will be discussed in this paper. The tumour structure is heterogeneous: tumour cells in close proximity to blood vessels proliferate rapidly in the presence of abundant oxygen and nutrients [5, 29], and where the rate of proliferation outstrips the rate of new blood vessel formation, transient areas of hypoxia form. The blood vessels in such tumours fall into two categories [27]: co-opted vessels that were originally part of the host's vascular network; and the neovasculature formed by the growth of small vessels into and within the tumour. Co-opted vessels have different properties from the angiogenic neovasculature. They have a fully-developed basal lamina, which makes them much stronger and more rigid than the new blood vessels. They also tend to be regularly spaced. By contrast, the neovasculature is immature, leaky and tortuous. Being immature, the neovasculature is only able to withstand relatively small increases in pressure, and, so, increases in the pressure exerted by tumour cells on blood vessels can cause their compression [6, 12, 29] or collapse, reducing, or halting, the supply of oxygen and nutrients to the surrounding region.

Vascular tumours consist of a mixture of cell types, including live and dead tumour cells, macrophages and endothelial cells lining the blood vessels, all embedded in an extracellular matrix. Cells attach themselves to the extracellular matrix by expressing proteins and other molecules on their surface which bind to complementary molecules in the matrix [1]. They also attach to one another. Collectively, these connections ensure the integrity of the tumour. The movement of cells within the extracellular matrix requires the formation of new contacts with the matrix and neighbouring cells, and the breaking of old contacts. Since dead cells are unable to make or retain such contacts, it is easier for them to move in response to physical cues (for example, changes in pressure within the tumour).

There have been numerous mathematical models of avascular tumour growth, see [11, 28] for example. Such models normally prescribe the oxygen tension at the proliferating rim and may involve 'compartmentalising' the tumour into proliferating, quiescent and necrotic regions. There have also been several studies of angiogenesis (see Anderson & Chaplain [2] and Byrne [8]). However, only a small amount of (mathematical) literature concerns the growth of vascular tumours. Macroscale models [7, 13, 23, 26] have been generated to describe various tumour phenomena: Sleeman & Nimmo [26] generate a model that describes how fluid moves out through the tumour's periphery; Orme & Chaplain [23] allow cell motion by diffusion and by taxis up gradients of capillary vessels, and they calculate the density of live tumour cells and the surface area of the capillary vessels per unit volume; Byrne & Chaplain [7] study the distribution of a blood-borne nutrient and an blood-borne inhibitor in a vascularised tumour, where the effects of the

vasculature are modelled by introducing distributed source terms into the equations for the nutrient and inhibitor; Hahnfeldt *et al.* [13] compare the predictions of a model describing the change in tumour volume with experimental tumour growth data. They include a variable ‘carrying capacity’, which changes with variations in the vasculature and with administered angiogenesis inhibitors (such as endostatin).

There are also several mathematical models that focus on the behaviour at a microscopic level [3, 21]. These are based on extensions to the Krogh Cylinder model [17], which describes the oxygen tension supplied from capillaries to the surrounding tissue. In Maseide & Rofstad [21], for example, two geometries are considered: a single vessel surrounded with tumour cells, and a capillary network surrounding an area of tumour cells. Space is compartmentalised so that there is a region where cells proliferate and a necrotic region (at distance from the vessel) where they do not. However, the cell density is taken to be spatially and temporally constant in each of the compartments: cell motion is assumed to act in such a way to keep the densities constant. Thus the number of cells entering the necrotic region is equal to the number generated in the proliferating zone. The ‘hypoxic fraction’ of the tumour mass (that is, the ratio of the hypoxic cell lifetime to the time required for the tumour segment to double its original volume when there is no cell loss) is calculated for various times, and various values of the hypoxic timescale and cell doubling timescale. The oxygen profile is also generated.

The flow of blood in collapsible tubes has been widely studied [20, 24]. For example, Luo & Pedley [20] model flow along pipes with a compliant wall, and consider the effects of wall inertia (which they find can be ignored when modelling blood flow in a collapsible pipe).

In this paper, we present a mathematical model to describe the behaviour of live and dead cells<sup>1</sup> residing between two identical compliant blood vessels that are fixed in space (see Figure 1). Our ‘microenvironment’ is large enough that the cellular matter may be viewed as a continuum, but small enough that we need focus on only one vessel, the microenvironment surrounding the second vessel being identical to that surrounding the first, reflected in the line of symmetry between the two. For simplicity, we restrict attention to one-dimensional models, with the spatial dimension being outward from the blood vessel. We solve the model numerically and examine the behaviour of the system as the key parameters are altered. Our model differs from the existing mathematical literature in a number of ways. The main differences are that (i) we are looking on a microscale within a vascular tumour, and we allow interactions between the blood vessel that supplies oxygen to the region and the tumour cells adjacent to it, (ii) we allow both live and dead cells to move, but at different speeds (the live cells move more slowly due to their pinning to the extracellular matrix), and (iii) we consider a compliant blood vessel.

In §2 we derive the underlying model which governs the evolution of the densities of live and dead cells, the oxygen tension, the cell speeds and the thickness of the blood vessel. In §3 we analyse the model for some special cases. In §4 we present numerical simulations of the governing equations, showing how the density of live cells, oxygen tension and cell speed change with time. We then vary the key parameters and show how

<sup>1</sup> We assume that only the densities of the live and dead cell components of the tumour vary. We comment on allowing variations in the volumetric component of extracellular water in §6.

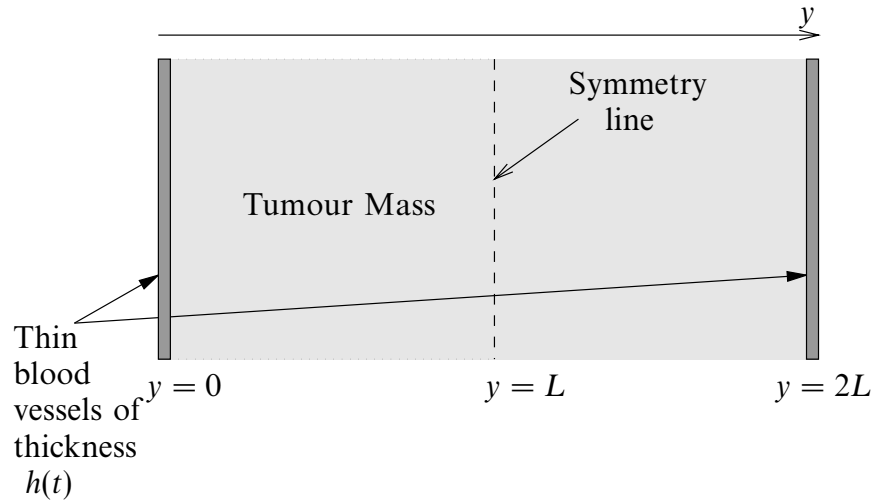


FIGURE 1. Domain under consideration.

they alter the long time behaviour of the system. In §5 we draw together the results of §3 and §4. Finally, in §6 we summarise the conclusions of the work and discuss extensions to the model together with clinical implications.

## 2 Mathematical model

We assume that the microenvironment within a tumour consists of a mixture of live and dead tumour cells, macrophages, extracellular water and endothelial cells (forming the tumour vasculature) embedded in a tissue matrix. The live tumour cells proliferate if the local oxygen tension is high enough, and the rate at which proliferation occurs is assumed to be proportional to both the local oxygen tension and the (number) density of live cells. We assume that live cells can die by two processes. The first, apoptosis [1], is programmed cell death ('old age') and occurs at all oxygen tensions. The rate of apoptosis may increase with decreasing oxygen tension [15], but in this model we assume it is proportional to the local density of live cells and independent of the local oxygen tension (we discuss relaxing this assumption in §6). The second death mechanism we consider is oxygen-induced-necrosis (henceforth termed 'necrosis'), which we assume here to be cell death induced by oxygen starvation ('suffocation'). The rate of such necrosis is assumed to be proportional to the local density of live cells and to be induced only when the oxygen tension drops below a threshold value. Other forms of necrotic cell death occur at all oxygen tensions, for example, necrosis due to low pH [4]: we stress that we do not consider such mechanisms in this paper. When live cells die by apoptosis, they become inactive but retain their form until they are either degraded by enzymes in the matrix or phagocytosed by macrophages (a type of stromal cell that moves around the tumour and accumulates in hypoxic areas) [19]. We suppose that these processes (which together we call degradation<sup>2</sup>) occur at a rate proportional to the local density of dead cells.

<sup>2</sup> We do not track the population of macrophages in the tumour.

As described above, the tumour mass comprises a mixture of cells other than live and dead tumour cells. One of the main differences between tumour cells and other cells is that tumour cells proliferate far more readily. Thus on the tumour proliferation timescale we may assume that the population of these ‘stromal’ cells remains constant and that their only effect is to consume oxygen.

Given that the main cellular component is water, we may assume that cells are incompressible. As a result, since we assume that the density of the stromal component remains constant, and that the cells pack space without any voids, the combined local density of live and dead cells together must also remain constant (as in Ward & King [28]). Since our blood vessels are fixed in space, the microenvironment does not increase in size. This has the immediate consequence that the increase in the *total* mass of live cells due to proliferation must exactly balance the *total* decrease in the mass of dead cells due to degradation. We discuss relaxing these assumptions in §6.

A cell requires sufficient oxygen, nutrients and cellular building blocks to reproduce. In this paper, we assume that the nutrients and building blocks are present in sufficient quantities throughout the tumour mass, and we merely keep account of the oxygen tension. The level of oxygen in tumour tissue depends on the spacing of the blood vessels and their thickness [14]. Since the oxygen supply is directly related to the number of red blood cells that can pass through the vessel, wider vessels typically supply greater levels of oxygen than thinner vessels. Once it extravasates, oxygen is consumed by the live cells, which use it to remain alive, proliferate (if the levels are high enough) and migrate. The rate at which cells consume oxygen is assumed to depend on the number of cells present and the local oxygen tension.

Cell proliferation and degradation in local sites throughout the tumour mass cause pressure gradients to be established. These, in turn, cause the blood vessel to open or close, and drive the movement of the live and dead cells. In this way the supply oxygen tension may vary due to changes in the local densities of the two cell types.

We denote the density of live tumour cells by  $n$ , the density of dead tumour cells by  $m$  and the oxygen tension by  $C$ . We let the live cells move with velocity  $v_n$  and the dead cells move with velocity  $v_m$ . Using conservation of mass, we formulate the following equations to describe the evolution of the densities of live and dead tumour cells:

$$\frac{\partial n}{\partial t} + \frac{\partial(v_n n)}{\partial y} = \underbrace{\lambda n C \mathcal{H}(C - C_1)}_{\text{Proliferation}} - \underbrace{An}_{\text{Apoptosis}} - \underbrace{Nn \mathcal{H}(C_2 - C)}_{\text{Necrosis}}, \tag{2.1}$$

$$\frac{\partial m}{\partial t} + \frac{\partial(v_m m)}{\partial y} = \underbrace{An}_{\text{Apoptosis}} + \underbrace{Nn \mathcal{H}(C_2 - C)}_{\text{Necrosis}} - \underbrace{Fm}_{\text{Degradation}}. \tag{2.2}$$

In (2.1) and (2.2),  $\lambda$  is the proliferation rate,  $C_1$  is a threshold oxygen tension below which proliferation does not occur ( $\mathcal{H}$  is the Heaviside function),  $A$  is the apoptosis rate,  $N$  is the necrosis rate,  $C_2$  is a threshold oxygen tension below which necrosis occurs,  $F$  is the dead cell degradation rate,  $y$  denotes the distance ‘outwards’ from the blood vessel and  $t$  denotes time. In (2.1) and (2.2), we have also assumed that a live cell and a dead cell have the same volume. We note that when  $C > C_1$  cells undergo proliferation and apoptosis. When  $C_1 > C > C_2$  cells undergo apoptosis only, and when  $C < C_2$

cells undergo apoptosis and necrosis. We remark further that, since the proliferation rate depends on the local nutrient concentration, and since the local nutrient concentration depends on the density of live cells (see equation (2.4) below), (2.1) does not automatically produce exponential tumour growth.

Since the total cell density remains constant, we have a further equation relating  $n$  and  $m$ , namely

$$n + m = M, \quad (2.3)$$

where  $M$  is the (constant) density of live and dead cells at an arbitrary point within the tumour mass. A conservation of mass equation could also be formulated for the evolution of the density of the stroma. Since we assume that this density is constant throughout the tumour mass, the equation would tell us the speed with which this component moved.

We use conservation of mass to generate the equation governing the evolution of the oxygen tension  $C$  in the tumour. We assume that changes in  $C$  are due to advection, diffusion and consumption, and so the resulting equation reads

$$\frac{\partial C}{\partial t} + \frac{\partial}{\partial y}(v_{av}C) = \underbrace{D \frac{\partial^2 C}{\partial y^2}}_{\text{Diffusion}} - \underbrace{E_1 n C}_{\text{Consumption by live tumour cells}} - \underbrace{E_2 C}_{\text{Consumption by stroma}}. \quad (2.4)$$

In (2.4),  $D$  is the diffusivity,  $E_1$  is the rate at which live tumour cells consume oxygen and  $E_2$  is the rate at which stromal cells consume oxygen. We have assumed, for simplicity, that oxygen advects with the (linear) phase averaged velocity,  $v_{av}$ , where

$$v_{av} = \frac{nv_n + mv_m}{n + m}. \quad (2.5)$$

The precise form for the advection velocity is immaterial, since, as we will see later in this section, in situations of practical interest the nondimensionalised leading order version of (2.4) is dominated by diffusion.

We suppose that the intratumour pressure causes movement of the cells towards areas of low pressure, and that the live cells are pinned more firmly to the extracellular matrix than the dead cells. Thus we have

$$v_m = -\sigma_1 \frac{\partial P}{\partial y}, \quad (2.6)$$

$$v_n = -\sigma_2 \frac{\partial P}{\partial y}, \quad (2.7)$$

where  $P$  is the pressure,  $\sigma_{1,2}$  are the motility coefficients, and  $\sigma_2 < \sigma_1$ . These relationships are applications of ‘Darcy’s Law’, an empirical law which relates liquid velocity to pressure within a porous medium [22].

Taken together, (2.1)–(2.4) define the evolution of the variables  $n$ ,  $m$ ,  $C$  and  $P$  on the moving domain  $h(t) \leq y \leq L$ ,  $t \geq 0$ , where  $h(t)$  is the thickness of the blood vessel. In these equations the cell speeds  $v_n$  and  $v_m$  are defined in terms of the pressure  $P$  by (2.6), (2.7). To close the system, we now couple (2.1)–(2.4) with the following initial and boundary conditions.

We suppose that changes in the blood vessel thickness are directly due to changes in

the pressure within the tumour<sup>3</sup>, by setting

$$P_B - P(h, t) = k(h(t) - h_B), \quad (2.8)$$

at the vessel wall. In (2.8),  $P_B$  is the pressure that the blood exerts on the vessel (assumed constant due to our one-dimensional geometry),  $h$  is the vessel thickness,  $h_B$  is the thickness of the vessel when there is no extra pressure applied by the surrounding tissue (i.e. when  $P(h, t) = P_B$ ), and  $k$  represents the stiffness of the vessel wall. Thus if the pressure in the tissue is greater than the pressure in the blood, the thickness of the vessel decreases from  $h_B$ . As described earlier, we suppose that the oxygen tension at the blood vessel is proportional to its thickness, so

$$C(h, t) = \frac{1}{\alpha}h(t), \quad (2.9)$$

where  $\alpha$  is the ‘supply constant’. We combine (2.8) and (2.9) to give

$$P_B - P(h, t) = k(\alpha C(h, t) - h_B). \quad (2.10)$$

We impose the following initial and boundary conditions on the tumour tissue. The initial density of live cells (and hence the density of dead cells) is prescribed. We assume the average cell speed  $v_{av}$  at the vessel wall  $y = h$  matches the wall speed, and no flow of cells across the line of symmetry out at  $y = L$  (see Figure 1). We also assume symmetry of the oxygen tension about the symmetry line. These conditions are equivalent to prescribing

$$n = n_0, \quad \text{at} \quad t = 0, \quad (2.11)$$

$$m = M - n_0, \quad \text{at} \quad t = 0, \quad (2.12)$$

$$v_{av} = \frac{\partial h}{\partial t} \quad \text{at} \quad y = h, \quad (2.13)$$

$$v_n = v_m = 0 \quad \text{at} \quad y = L, \quad (2.14)$$

$$\frac{\partial C}{\partial y} = 0 \quad \text{at} \quad y = L, \quad (2.15)$$

where  $n_0$  is the initial density of live cells.

We are now in a position to nondimensionalise the model. Since we are interested in interactions between tumour cells and the blood vessel, we scale time with the tumour cell proliferation timescale ( $\lambda C_0$ ). We scale lengths with half the intervascular distance (i.e. with  $L$ ), the live and dead cell densities with the initial total density of cells ( $M$ ), and we scale the oxygen tension with the oxygen that would be supplied by a vessel of width  $h_B$  ( $C_0 = h_B/\alpha$ ). Further, we scale the thickness of the vessel with its undisturbed thickness ( $h_B$ ), and we scale the pressure difference from the blood pressure with  $kh_B$ . Thus, using primes to denote dimensionless variables, we set

$$\begin{aligned} n &= Mn', & m &= Mm', & C &= \frac{h_B}{\alpha}C', & v_{n,m} &= \frac{\lambda h_B L}{\alpha}v'_{n,m}, \\ t &= \frac{\alpha}{\lambda h_B}t', & y &= Ly', & h &= h_B h', & P &= P_B + kh_B P'. \end{aligned} \quad (2.16)$$

We eliminate  $v_n$  and  $v_m$  from (2.1), (2.2) and (2.4), and the resulting nondimensionalised

<sup>3</sup> Strictly speaking, it is the curvature of the blood vessel that changes as the pressure changes – see Luo & Pedley [20]. We choose (2.8) for simplicity since we are working in one spatial dimension.

system of equations and boundary conditions reads (dropping primes)

$$\frac{\partial n}{\partial t} - \delta \sigma^* \frac{\partial}{\partial y} \left( n \frac{\partial P}{\partial y} \right) = n c \mathcal{H}(C - C_1^*) - A^* n - N^* n \mathcal{H}(C_2^* - C), \quad (2.17)$$

$$\frac{\partial m}{\partial t} - \sigma^* \frac{\partial}{\partial y} \left( m \frac{\partial P}{\partial y} \right) = A^* n + N^* n \mathcal{H}(C_2^* - C) - F^* m, \quad (2.18)$$

$$n + m = 1, \quad (2.19)$$

$$Pe \left( \frac{\partial C}{\partial t} - \sigma^* \frac{\partial}{\partial y} \left( (m + \delta n) C \frac{\partial P}{\partial y} \right) \right) = \frac{\partial^2 C}{\partial y^2} - E_1^* n C - E_2^* C, \quad (2.20)$$

with

$$n = n_0, \quad \text{at} \quad t = 0, \quad (2.21)$$

$$P + C = 1, \quad \text{at} \quad y = \epsilon h, \quad (2.22)$$

$$-\sigma^* (m + \delta n) \frac{\partial P}{\partial y} = \epsilon \frac{\partial h}{\partial t} \quad \text{at} \quad y = \epsilon h, \quad (2.23)$$

$$\frac{\partial P}{\partial y} = 0 \quad \text{at} \quad y = 1, \quad (2.24)$$

$$\frac{\partial C}{\partial y} = 0 \quad \text{at} \quad y = 1. \quad (2.25)$$

The thickness of the blood vessel may be found using the dimensionless analogue of (2.9), namely

$$h(t) = C(0, t). \quad (2.26)$$

The nondimensional parameter groups introduced into (2.17)–(2.26) are defined below as

$$A^* = \frac{A}{\lambda C_0}, \quad N^* = \frac{N}{\lambda C_0}, \quad F^* = \frac{F}{\lambda C_0}, \quad \epsilon = \frac{h_B}{L},$$

$$C_1^* = \frac{C_1}{C_0}, \quad C_2^* = \frac{C_2}{C_0}, \quad Pe = \frac{\lambda C_0 L^2}{D}, \quad (2.27)$$

$$E_1^* = \frac{E_1 M L^2}{D}, \quad E_2^* = \frac{E_2 L^2}{D}, \quad \delta = \frac{\sigma_1}{\sigma_2}, \quad \sigma^* = \frac{\sigma_2 \alpha k}{\lambda L^2}.$$

Before summarising our mathematical model we now estimate that two of the parameters are small:

- $\epsilon \sim 0.02 \ll 1$ , for blood vessels of width  $h_B = 10 \mu\text{m}$  and a tumour intervascular distance of 1 mm (so that  $L = 5 \times 10^{-4}$  m).
- $Pe \sim 0.03 \ll 1$ , for diffusivity  $D \sim 10^{-10} \text{ m}^2 \text{ s}^{-1}$ , and with a proliferation timescale of 1 day ( $\lambda C_0 \sim 10^5$  s).

Thus, we take the limits  $\epsilon \rightarrow 0$ ,  $Pe \rightarrow 0$ , with consequences that the blood vessel boundary conditions are applied on  $y = 0$ , the speed of the cells at the blood vessel wall is zero, and the problem for the oxygen tension becomes quasi-steady.

### Summary of model equations

Taken together, (2.17)–(2.20) define  $n$ ,  $m$ ,  $P$  and  $C$ . It is convenient to use (2.19) to eliminate either  $n$  or  $m$  from the model. Eliminating  $m = 1 - n$  between (2.17)–(2.18) and taking the limits  $\epsilon, Pe \rightarrow 0$ , our model may be summarised as

$$\frac{\partial n}{\partial t} - \left( \frac{\sigma^* \delta}{1 - (1 - \delta)n} \right) \frac{\partial n}{\partial y} \frac{\partial P}{\partial y} = \frac{n(1 - n) [C \mathcal{H}(C - C_1^*) + F^* \delta]}{1 - (1 - \delta)n} - [A^* + N^* \mathcal{H}(C_2^* - C)] n, \quad (2.28)$$

$$-\sigma^* \frac{\partial}{\partial y} \left( (1 - (1 - \delta)n) \frac{\partial P}{\partial y} \right) = nC \mathcal{H}(C - C_1^*) - F^*(1 - n), \quad (2.29)$$

$$\frac{\partial^2 C}{\partial y^2} = E_1^* nC + E_2^* C, \quad (2.30)$$

with initial and boundary conditions

$$n = n_0, \quad \text{at} \quad t = 0, \quad (2.31)$$

$$P + C = 1, \quad \text{at} \quad y = 0, \quad (2.32)$$

$$\frac{\partial P}{\partial y} = 0 \quad \text{at} \quad y = 0, 1, \quad (2.33)$$

$$\frac{\partial C}{\partial y} = 0 \quad \text{at} \quad y = 1. \quad (2.34)$$

The width of the blood vessel is determined *a posteriori* using

$$h(t) = C(0, t). \quad (2.35)$$

Thus, our model comprises two second-order linear ordinary differential equations (for  $C$  and  $P$ ) which are coupled to a nonlinear hyperbolic partial differential equation (for  $n$ ).

## 3 Explicit solutions

In this section, we use our mathematical model to develop a number of useful identities. The first set of results will be useful for understanding the initial behaviour of the system (and thus form the basis for validating our numerical solutions). By studying the initial solutions we also gain insight into how the parameters influence the behaviour of the system. The identities in §3.2–3.4 will be useful for characterising the way in which the long-time behaviour of the system varies with key model parameters, and will be used in §5 where the numerical solutions of §4 are discussed.

### 3.1 Initial oxygen tension and pressure profiles

In this subsection we determine the initial profiles for the oxygen tension and the pressure, given that  $n = n_0$ . For simplicity we set  $E_2^* = 0$  (i.e. the stromal cells consume negligible amounts of oxygen). We consider the three different cases that may arise in turn. The different cases correspond to  $C(y, 0) > C_1^*$  everywhere,  $C(0, 0) > C_1^* > C(1, 0)$  and

$C(y, 0) < C_1^*$  everywhere separately. In practice, the case that is realised depends on the parameter values. However, we do not know, *a priori*, which parameter regimes give rise to a particular case.

*Case 1:*  $C(y, 0) > C_1^* \forall y \in [0, 1]$

If  $C > C_1^*$  everywhere (i.e. there is sufficient oxygen present for proliferation to occur throughout the tumour mass), then (2.30), with boundary condition (2.34), yields

$$C = a_1 \cosh [B_r(1 - y)], \quad (3.1)$$

where  $B_r = \sqrt{E_1^* n_0}$ . We substitute (3.1) into (2.29) which, after applying  $\partial P / \partial y = 0$  at  $y = 0, 1$  gives

$$[1 - (1 - \delta)n_0] \frac{\partial P}{\partial y} = -\frac{F^*}{\sigma^*}(1 - n_0)(1 - y) + \frac{a_1}{\sigma^*} \sinh [B_r(1 - y)], \quad (3.2)$$

where

$$a_1 = \frac{F^*(1 - n_0)B_r}{n_0 \sinh B_r}. \quad (3.3)$$

We note that the solutions for  $C$  and  $\partial P / \partial y$  were obtained by using (2.33) and (2.34). In practice, (3.2) is used to fix the arbitrary constant of integration which arises when solving (3.2) for  $P$ . The solutions for  $C$  and  $v_m (= \partial P / \partial y)$  then read

$$C = \frac{F^*(1 - n_0)B_r \cosh B_r(1 - y)}{n_0 \sinh B_r}, \quad (3.4)$$

$$-\sigma^* \frac{\partial P}{\partial y} = v_m = \frac{F^*(1 - n_0)}{1 - (1 - \delta)n_0} \left( 1 - y - \frac{\sinh B_r(1 - y)}{\sinh B_r} \right) \geq 0. \quad (3.5)$$

We note that case 1 pertains if  $C(1, 0) > C_1^*$ , i.e. if

$$\frac{F^*(1 - n_0)B_r}{n_0 \sinh B_r} \geq C_1^*. \quad (3.6)$$

Using (3.4) and (3.5), we can easily see that the speed  $v_m$  is non-negative everywhere and has a unique internal maximum, and that the oxygen tension is monotonic decreasing. The physical interpretations are that tumour cells move outward from the blood vessel into the tumour mass, and that the oxygen tension is progressively reduced due to cell consumption. We can also use (2.35) and (3.4) to determine the initial thickness of the blood vessel:

$$h(t = 0) = F^*(1 - n_0) \frac{B_r}{n_0} \coth B_r. \quad (3.7)$$

Thus, specifying the initial density of live cells, so that  $n = n_0$  at  $t = 0$ , automatically dictates the initial thickness of the blood vessel. In particular, the initial density of live cells and the blood vessel thickness cannot be prescribed independently. We note also that the vessel thickness depends upon the cell degradation rate  $F^*$  but not on the apoptosis rate  $A^*$ . This is to be expected, since  $F^*$  describes net volume loss from the system, whereas  $A^*$  does not. Finally, in the limit  $E_1^* \rightarrow 0$ ,  $h(0) \rightarrow F^*(1 - n_0)/n_0$ .

Case 2:  $C(y, 0) > C_1^*$  for  $0 \leq y \leq y_p \leq 1$ , where  $C(y_p) = C_1^*$

We now consider the case where  $C$  passes through the threshold  $C_1^*$  at a point  $y = y_p \in (0, 1)$  in the tumour mass, so that  $C(y_p) = C_1^*$ . In this case, the oxygen tension is given by

$$C = \frac{F^*(1 - n_0)B_r \cosh[B_r(1 - y)]}{n_0 (\sinh B_r - \sinh[B_r(1 - y_p)])}, \tag{3.8}$$

the cell speed satisfies

$$v_m = \begin{cases} -\frac{F^*(1-n_0)y}{(1-(1-\delta)n_0)} + \frac{F^*(1-n_0)(\sinh[B_r(1-y)]-\sinh B_r)}{(1-(1-\delta)n_0)(\sinh[B_r(1-y_p)]-\sinh B_r)} & \text{if } y < y_p, \\ \frac{F^*(1-n_0)(1-y)}{(1-(1-\delta)n_0)} & \text{if } y > y_p, \end{cases} \tag{3.9}$$

and  $y_p$  solves

$$\frac{\cosh[B_r(1 - y_p)]}{\sinh B_r - \sinh[B_r(1 - y_p)]} = \frac{C_1^* n_0}{F^*(1 - n_0)B_r}. \tag{3.10}$$

We note that equation (3.10) defines whether a Case 2 solution exists. In particular, if (3.10) possesses a root  $y_p$  such that  $0 \leq y_p \leq 1$  then a Case 2 solution will be realised.

Case 3:  $C(y, 0) < C_1^* \forall y \in [0, 1]$

The final case we consider arises when  $C < C_1^*$  everywhere. As noted in the introduction, when operating on a fixed domain, the total increase in mass of live cells due to proliferation must balance the total decrease in mass of dead cells due to degradation. Thus, Case 3, where no proliferation occurs, may only arise when there is no degradation, *i.e.*  $n_0 = 1$  or  $F^* = 1$  from (2.29). In this case,  $\partial P / \partial y = 0$  everywhere (*i.e.*  $v_m = 0$ ), and the solution reads

$$C = a_1 \cosh B_r(1 - y), \quad P = 1 - a_1 \cosh B_r, \tag{3.11}$$

with  $a_1 < C_1^* / \cosh B_r$  undetermined. To understand why the solution is not uniquely defined, it is instructive to consider the coupling between  $P$  and  $C$ . When  $C > C_1^*$  equation (2.29) translates information about  $\partial P / \partial y$  at  $y = 0$  into information about  $\partial C / \partial y$  at  $y = 0$  and enables a unique solution for  $C$  to be determined (note that, as stated previously, (2.32) provides information about the constant of integration needed to uniquely specify the pressure,  $P$ ). For Case 3 solutions, the coupling between  $P$  and  $C$  in (2.29) is lost and, in consequence, we are unable to determine fully the solution for  $C$  (and, hence, for  $P$ ).

*Discussion*

In Figure 2, we show graphs of the oxygen tension  $C$  and the dead cell speed  $v_m$  for two choices of the tumour cell oxygen consumption rate  $E_1^*$ . The graphs reveal several important features:

- The change in the oxygen tension across the domain increases as  $E_1^*$  increases. This is to be expected since  $C(1, 0) = C(0, 0)\text{sech}B_r$ , where  $B_r = \sqrt{E_1^*n_0}$ , and so

$$\Delta C(t = 0) = C(0, 0) - C(1, 0) = (1 - \text{sech}B_r)C(0, 0) \tag{3.12}$$

which increases as  $E_1^*$  increases.

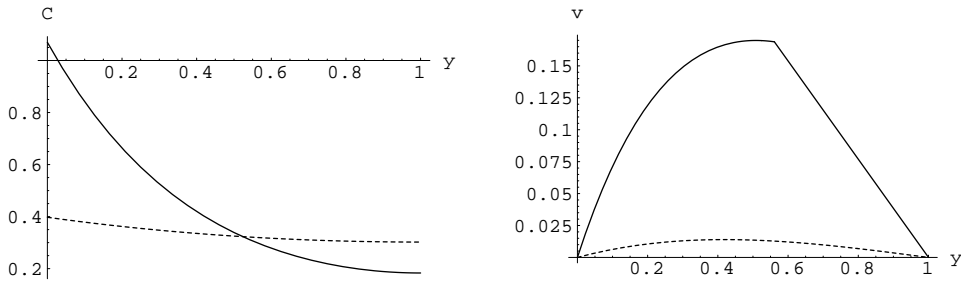


FIGURE 2. Graphs showing (a) the oxygen tension and (b) the cell speed for  $E_1^* = 1$  (dotted) and  $E_1^* = 10$  (solid). Here  $F^* = 0.5$ ,  $\delta = 0.2$ ,  $n_0 = 0.6$  and  $C_1^* = 0.3$ .

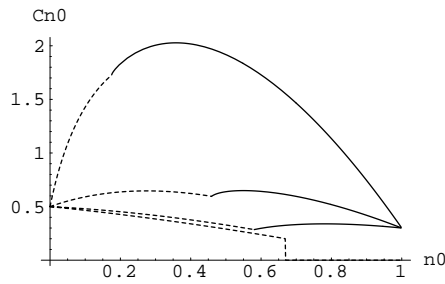


FIGURE 3. Graph showing how the proliferation rate at the blood vessel  $n_0C(0)$  changes with the initial density of live cells  $n_0$ , for various fixed values of the consumption rate  $E_1^* = 1$  (lowest line),  $E_1^* = 2$ ,  $E_1^* = 10$  and  $E_1^* = 100$  (highest line). Dotted portions indicate areas where  $C > C_1^*$  everywhere and solid lines indicate areas where  $C(0) > C_1^* > C(1)$ .

- When  $E_1^* = 1$ ,  $C > C_1^*$  everywhere, but when  $E_1^* = 10$ ,  $C(0) > C_1^* > C(1)$ .
- When  $E_1^* = 1$ , the dead cell speed profile is smooth whereas when  $E_1^* = 10$ , there is a jump in the slope of  $v_m$  which coincides with proliferation switching off (i.e. when  $C = C_1^*$ ).

We note that our model does not admit solutions for which  $n_0 = 0$ . Indeed, it adjusts to keep the live cell density positive. We can see this by considering the behaviour of  $C(0)$ . Using (3.4) and (3.8), we deduce that as  $n_0 \rightarrow 0$ ,  $C(0) \rightarrow \infty$ . However, the initial proliferation rate  $n_0C(0)$  remains finite as  $n_0 \rightarrow 0$  (in fact  $n_0C(0) \rightarrow F^*$ ). We demonstrate this result in Figure 3, where we sketch the proliferation rate for various values of  $E_1^*$ . Referring to Figure 3, we note in passing that several values of  $n_0$  may yield the same value for the proliferation rate.

### 3.2 Variation of the total live cell population

We are able to determine the evolution of the total number of live cells in the region, providing  $C > C_2^*$  everywhere. Defining

$$\mathcal{N}(t) = \int_0^1 n(y, t) dy, \tag{3.13}$$

we integrate (2.18)<sup>4</sup> across the tumour mass to obtain

$$\mathcal{N}'(t) + (A^* + F^*)\mathcal{N} = F^*. \quad (3.14)$$

(3.14) has the solution

$$\mathcal{N} = \frac{F^*}{A^* + F^*} + \left( n_0 - \frac{F^*}{A^* + F^*} \right) e^{-(A^* + F^*)t}. \quad (3.15)$$

Thus,

$$\mathcal{N} \rightarrow \frac{F^*}{A^* + F^*} \quad \text{as} \quad t \rightarrow \infty. \quad (3.16)$$

We see that increasing  $F^*$  increases the final value of  $\mathcal{N}$ . This is because increasing the degradation rate removes dead cells more quickly from the system and, thus, to compensate, the live cell population must increase to ensure that the available space remains filled. Conversely, decreasing the apoptosis rate enables cells to remain alive for longer and, hence, increases  $\mathcal{N}$ . We note that  $\mathcal{N}$  is independent of  $E_1^*$  and  $\delta$ .

When  $C$  falls below  $C_2^*$  somewhere in the tumour mass, the relationship for  $\mathcal{N}$  as  $t \rightarrow \infty$  reads

$$\mathcal{N} \rightarrow \frac{F^*}{A^* + F^* + N^*} + \frac{N^*}{A^* + F^* + N^*} \int_0^{y_N} ndy, \quad (3.17)$$

where  $y_N$  is such that  $C(y_N, t) = C_2^*$ . This relationship is less useful than (3.16) since it contains the unknown factor  $\int_0^{y_N} ndy$ .

### 3.3 Variation of the total amount of oxygen consumed

We now derive an expression for the total amount of oxygen being consumed within the tumour at time  $t$ . Substitution from (2.30) into (2.17) and then integration across the tumour mass yields

$$\mathcal{N}'(t) + A^*\mathcal{N} = -\frac{1}{E_1^*}C_y|_0, \quad (3.18)$$

providing  $C > C_1^*$ . This equation shows how the gradient of oxygen tension at the origin varies with time, and, on substituting for  $\mathcal{N}(t)$ , may be rearranged to give

$$C_y|_0 = -E_1^* \left( \frac{A^*F^*}{A^* + F^*} - F^* \left( n_0 - \frac{F^*}{A^* + F^*} \right) e^{-(A^* + F^*)t} \right). \quad (3.19)$$

Thus, the problem has an intrinsic boundary condition for  $C$ , namely (3.19), which may be used in conjunction with (2.34) and (2.20) to obtain the oxygen tension.

We obtain a relationship for the total amount of oxygen being consumed by integrating (2.30) across the tumour mass and using (3.19). The result reads

$$\mathcal{C}(t) = E_1^* \int_0^1 nC dy = E_1^* \left( \frac{A^*F^*}{A^* + F^*} - F^* \left( n_0 - \frac{F^*}{A^* + F^*} \right) e^{-(A^* + F^*)t} \right). \quad (3.20)$$

Thus,

$$\mathcal{C} \rightarrow \frac{E_1^*A^*F^*}{A^* + F^*} \quad \text{as} \quad t \rightarrow \infty. \quad (3.21)$$

We see that increasing  $E_1^*$ ,  $A^*$  and  $F^*$  all increase the value of  $\mathcal{C}$ .

<sup>4</sup> It is easier to use the original equation for  $m$  to obtain (3.15).

### 3.4 The small oxygen consumption rate approximation

We can make substantial progress when both the consumption rates are small ( $E_1^*$ ,  $E_2^* \rightarrow 0$ ). In this limit, we set  $E_1^* = E_2^* = 0$  and the oxygen tension problem (2.20), (2.34) has the solution

$$C = C(t). \quad (3.22)$$

Note that we do not recover equation (3.19) in this limit because we are unable to substitute from (2.30) into (2.17). However, (2.29) may be integrated to give

$$-\sigma^* \frac{\partial P}{\partial y} = \frac{C(t) + F^*}{1 - (1 - \delta)n} \int_0^y n dy - \frac{F^* y}{1 - (1 - \delta)n}. \quad (3.23)$$

By applying boundary condition (2.33) at  $y = 1$ , we obtain a relationship between  $\mathcal{N}(t)$  and  $C(t)$ , namely

$$C(t) = \frac{F^* (1 - \mathcal{N}(t))}{\mathcal{N}(t)}. \quad (3.24)$$

We note that this relationship may also be obtained by integrating (2.17) and (2.18) and comparing the resulting expressions. Whenever  $E_1^*$ ,  $E_2^* \ll 1$ , (3.24) replaces the relationship for  $\partial C / \partial y|_0$  stated in (3.19). In such cases, (3.24) proves more useful than (3.19), since it enables us to determine whether the blood vessel expands. We use the long-time behaviour of  $\mathcal{N}$  given by (3.16) to find that

$$C_\infty = \lim_{t \rightarrow \infty} C(0, t) = A^*. \quad (3.25)$$

Since  $h(t) = C(0, t)$ , and  $C(0, 0) = F^*(1 - n_0)/n_0$ , we find that the vessel ultimately becomes constricted, compared to its original thickness, if

$$n_0 < \frac{F^*}{A^* + F^*}. \quad (3.26)$$

There is an natural physical interpretation of this result. If (3.26) holds, then the total live cell population increases (from (3.15)), and thus the vessel becomes constricted (since areas of proliferating cells correspond to areas of higher pressure within the tumour mass).

## 4 Numerical simulations

In this section we present numerical simulations of model equations (2.28)–(2.34). Before doing so, we make the following observations that guide our choice of several of the key dimensionless parameters:

- The rate of proliferation must exceed the rate of apoptosis, since tumour cells are, by definition, aggressive proliferators and so  $A^* < 1$  in (2.28).
- Standard biological dogma says that the ‘consumption distance’ of oxygen in tumour tissue is several hundred microns [5, 14]. Thus, we take  $\sqrt{D/E_1 M}$  to be  $O(100)$  microns.
- The hypoxic switch, below which cell proliferation ceases, corresponds to an oxygen tension of several *mmHg* and the switch to necrotic death occurs at a slightly lower oxygen tension. Thus we assume  $1 > C_1^* > C_2^*$ .
- Live cells are less motile than dead cells and so  $\delta \leq 1$  in (2.28) and (2.29).

We now make assumptions about the magnitudes of the necrosis rate and the degradation rate compared to the rate of proliferation. We suppose that necrosis occurs at a faster rate than proliferation and that degradation occurs at a similar rate to apoptosis, i.e.  $N^* > 1$  and  $F^* \sim A^*$ . Finally, we assume that the rate at which the stromal tissue consumes oxygen is negligible, so that  $E_2^* = 0$  in (2.30). Whilst these assumptions are based on discussions with biologists, there would be no adverse effects, from a mathematical viewpoint, if we fixed  $N^* < 1$ ,  $F^*$  larger or smaller than  $A^*$  or  $E_2^*$  nonzero. We proceed under the stated assumptions because we believe that they reflect, phenomenologically, the relative importance of the effects of degradation, necrosis and stromal consumption.

#### 4.1 Time-dependent solutions

In this section we present a typical set of time dependent solutions to (2.28–2.34). Our aim is to illustrate the gross physical features of the system and, to this end, we fix the parameters at the following representational values:

$$A^* = F^* = 0.5, \quad N^* = 2.0, \quad C_1^* = 0.3, \quad C_2^* = 0.2,$$

$$\sigma^* = 1, \quad E_1^* = 10, \quad E_2^* = 0, \quad \delta = 0.2, \quad n_0 = 0.6.$$

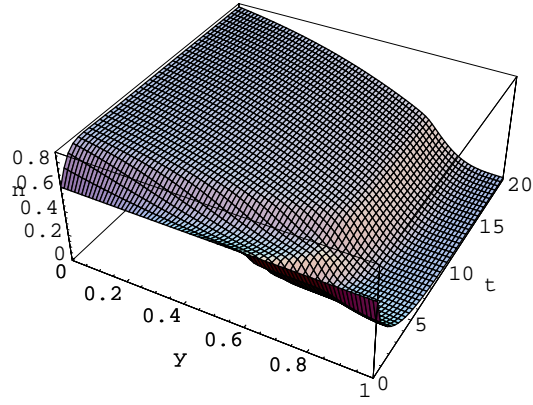
The general evolution of the tumour mass is depicted in Figure 4. First, we note that the initial profiles (as described in §3.1) are such that the oxygen tension decreases monotonically from the blood vessel. We have a case-2 initial condition, since  $y_p = 0.56$ . In fact, with this choice of parameters,  $C(1, 0)$  is slightly less than  $C_2^*$ , and necrosis occurs near to  $y = 1$ . Thus, initially, cells close to the blood vessel proliferate and the density of live cells there increases. Away from the vessel, the density of live cells decreases since apoptosis and necrosis outweigh proliferation. However, after a very short time ( $\sim t = 0.05$ ), the oxygen tension is everywhere above  $C_2^*$  and necrosis halts.

After the cells away from the blood vessel have died, they are degraded. This creates space away from the blood vessel. The live and dead cells produced closer to the vessel are pushed out into the tumour tissue and thus cell motion outward from the vessel is established. Being more motile, the dead cells migrate more readily than the live cells. This liberates more space for live cells close to the vessel to proliferate, and so their density there increases.

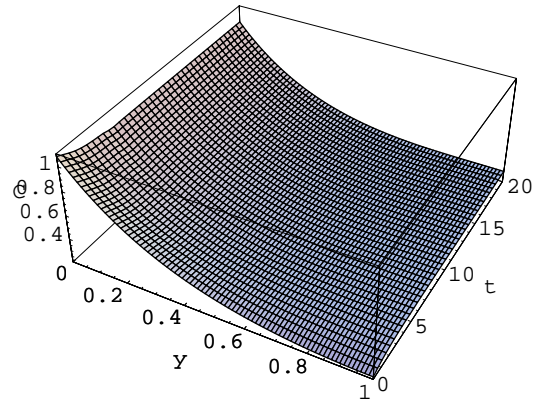
Pressure changes close to the vessel lead (in this case) to closure of the vessel and, thus, the supply oxygen tension (that is, the oxygen tension at the blood vessel wall) decreases. As the density of live cells away from the blood vessel decreases, the amount of oxygen consumed there also decreases, and so the overall oxygen tension away from the blood vessel rises.

We note that since (2.20), the equation for oxygen tension, is quasi-steady, small jumps in the oxygen tension may appear between consecutive timesteps. These jumps are associated with the motion of the hypoxic boundary along which  $C = C_1^*$ : they can be ‘smoothed out’ by replacing the Heaviside functions with smooth-but-steep counterparts (e.g. a *tanh* function).

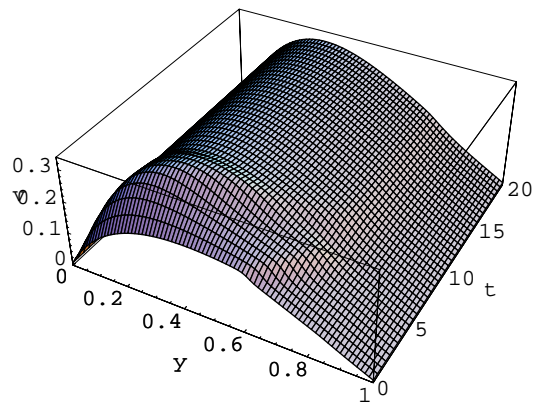
The simulations presented in Figure 4 suggest that the system may settle to a steady



(a)



(b)



(c)

FIGURE 4. Series of graphs showing the time-dependent development of the density of live tumour cells  $n(y, t)$ , the oxygen tension  $C(y, t)$  and the speed of dead cells  $v_m = v(y, t)$ .

state. In the following section, we examine how the steady state solution changes as the key parameters of the model are varied.

## 4.2 Steady state profiles

In this section we vary the individual model parameters, in order to assess their effects on the equilibrium spatial structure. In each case, we present steady state profiles for three values of the parameter, while keeping all the other parameters constant, and highlight the behaviour that we observe. We postpone the discussion of the behaviour until §5.

### 4.2.1 Oxygen consumption rate

Figure 5 shows the effect of varying the oxygen consumption rate  $E_1^*$  on the density of live cells, the oxygen tension, and the dead cell speed. It shows that increasing the oxygen consumption rate:

- generates a large area of dead cells away from the blood vessel (for sufficiently large  $E_1^*$ , the area of dead cells forms initially by necrosis and apoptosis (together) and is then sustained by the motion of dead cells into the region);
- increases the supply oxygen tension and decreases the tension away from the vessel;
- causes the average cell speed to increase and the peak speed to occur closer to the blood vessel.

We note that the largest density of live cells, which occurs at the origin, coincides with the largest supply oxygen tension, and the fastest speed of dead cells.

Finally, we note that qualitatively similar effects are obtained when the intercapillary distance is varied. This is to be expected, since the dimensionless group  $E_1^*$  is defined in terms of the dimensional parameters as  $E_1^* = E_1 ML^2/D$ . Since the lengthscale appears in other dimensionless parameter groupings, the behaviour observed when the intercapillary distance increases is not identical to that observed when the live cell oxygen consumption rate is increased. We conclude that if the distance between the vessels is small then the inter-vessel oxygen tension will be spatially independent and that a large intercapillary distance will generate an intermediate region of dead cells.

### 4.2.2 Apoptosis rate

Figure 6 shows the effect of varying the apoptosis rate  $A^*$  on the density of live cells, the oxygen tension, and the dead cell speed. Decreasing the apoptosis rate:

- increases the density of live cells close to the blood vessel, and decreases the density of live cells at distance from the vessel, generating a region consisting entirely of dead cells there;
- decreases the oxygen tension (throughout the tumour mass);
- increases the cell speed, and shifts the position at which the maximum speed occurs away from the blood vessel.

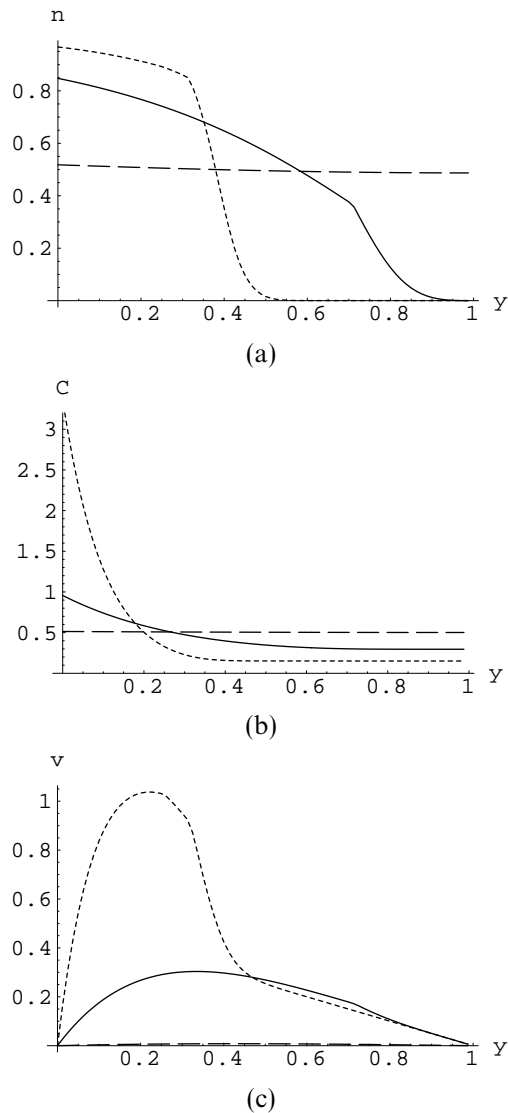


FIGURE 5. Series of graphs showing how the steady state profiles for (a)  $n$ , (b)  $C$  and (c)  $v = v_m$  change as the rate of oxygen consumption increases. Key:  $E_1^* = 0.1$  (dashed),  $E_1^* = 10$  (solid) and  $E_1^* = 100$  (dotted).

Comparing Figures 5 and 6, several key features become apparent. In both cases, as  $A^*$  and  $E_1^*$  increase, the maximum density of live cells, which occurs at the origin, and the maximum cell speed increase in magnitude. However, the supply oxygen tension increases with increasing  $E_1^*$  and decreases with increasing  $A^*$ . Further, as  $A^*$  increases the oxygen tension appears to increase at all points within the tumour mass whereas when  $E_1^*$  is increased the oxygen tension near the blood vessel increases and the oxygen tension at distance from the vessel decreases.

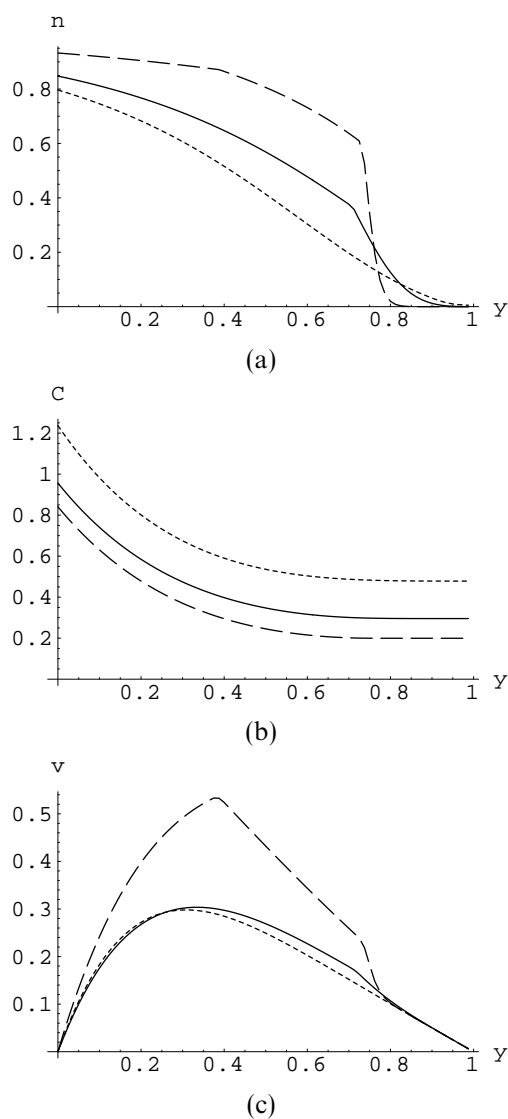


FIGURE 6. Series of graphs showing how the steady state profiles for (a)  $n$ , (b)  $C$  and (c)  $v = v_m$  change as the rate of apoptosis increases. Key:  $A^* = 0.25$  (dashed),  $A^* = 0.5$  (solid) and  $A^* = 0.75$  (dotted).

#### 4.2.3 Degradation rate

The effects of varying the degradation rate  $F^*$  on the steady state profiles of  $n$ ,  $C$  and  $v_m$  are presented in Figure 7. The graphs show that increasing the degradation rate:

- increases the density of live cells everywhere;
- increases the supply oxygen tension and decreases the oxygen tension away from the blood vessel;

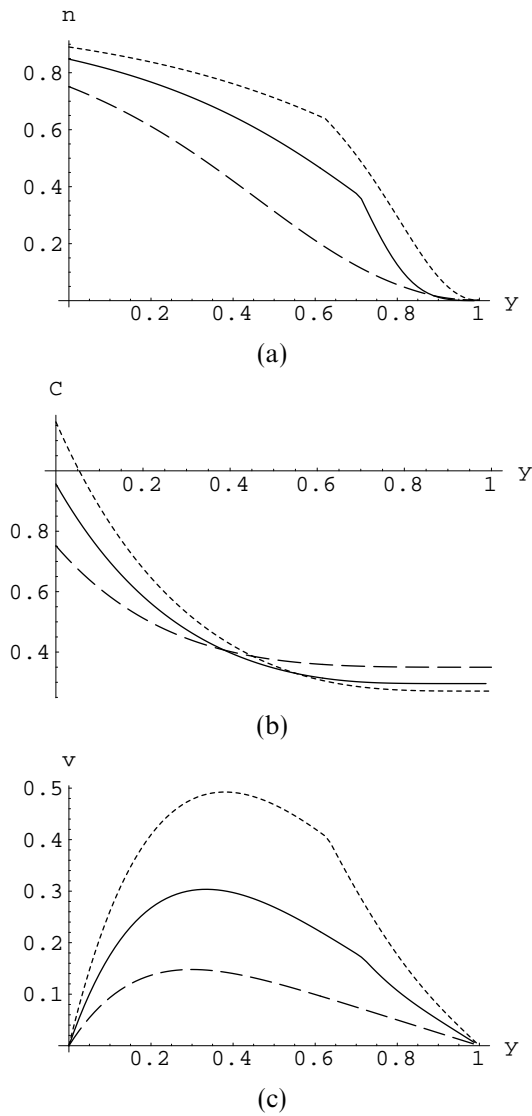


FIGURE 7. Series of graphs showing how the steady state profiles for (a)  $n$ , (b)  $C$  and (c)  $v = v_m$  change as the rate of degradation increases. Key:  $F^* = 0.25$  (dashed),  $F^* = 0.5$  (solid) and  $F^* = 0.75$  (dotted).

- increases the cell speed, and shifts the position at which the maximum occurs away from the blood vessel.

We note from Figure 7 that the density of live cells and the oxygen tension attain maxima at the blood vessel and that these maxima increase with increasing  $F^*$ . Additionally, the maximum dead cell speed increases with  $F^*$ . These features are qualitatively similar to those presented in Figure 5 ( $E_1^*$  varies), but differ from those of Figure 6 ( $A^*$  varies).

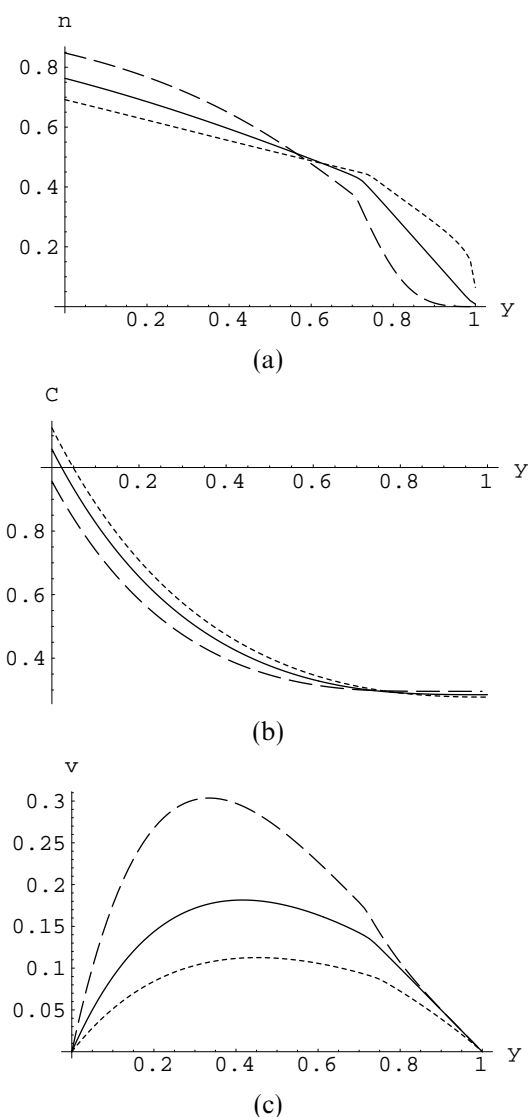


FIGURE 8. Series of graphs showing how the steady state profiles for (a)  $n$ , (b)  $C$  and (c)  $v = v_m$  change as the motility coefficient increases. Key:  $\delta = 0.2$  (dashed),  $\delta = 0.5$  (solid) and  $\delta = 1.0$  (dotted).

#### 4.2.4 Relative motility

We show the effects of varying the motility constant  $\delta$  on the steady state profiles of  $n$ ,  $C$  and  $v_m$  in Figure 8. Increasing  $\delta$

- decreases the density of live cells close to the blood vessel and increases the density away from the blood vessel;
- increases the supply oxygen tension;
- decreases the cell speed and shifts the position of the maximum away from the vessel.

Comparing Figures 6 and 8, we see that as  $\delta$  and  $A^*$  are increased, the maximum density of live cells corresponds to the lowest value of the supply oxygen tension, and the largest dead cell speed. This is in contrast to the behaviour shown in Figures 5 and 7 for changes in  $E_1^*$  and  $F^*$  respectively.

#### 4.2.5 Proliferation rate

Since the proliferation rate  $\lambda$  has been scaled out of the problem, in order to determine how variations in  $\lambda$  effect the system's evolution, we refer to (2.27) which shows that, as  $\lambda$  increases,  $A^*$ ,  $N^*$ ,  $F^*$  and  $\sigma^*$  decrease. We can see from (2.27) that all these parameters, other than  $\sigma^*$ , contain the scaling  $\lambda h_B/\alpha = \lambda C_0$ . We anticipate that if we increase  $\lambda$ , we may, by re-scaling the oxygen tension problem appropriately, recover our original problem. Thus, we consider two problems: one with parameters  $A^*$ ,  $N^*$ ,  $F^*$  and  $\sigma^*$  (with dependent variables  $n$ ,  $C$  and  $P$ ) and the second with parameters  $A^*/a$ ,  $N^*/a$ ,  $F^*/a$  and  $\sigma^*/a$  (with dependent variables  $\hat{n}$ ,  $\hat{C}$  and  $\hat{P}$ ), in order to simulate increasing the proliferation rate (where  $a$  is an arbitrary constant). Providing  $C > C_1^*$  for both problems, the steady state for the second problem reads

$$-\sigma^* \delta \frac{\partial}{\partial y} \left( \hat{n} \frac{\partial \hat{P}}{\partial y} \right) = a \hat{n} \hat{C} - A^* \hat{n}, \quad (4.1)$$

$$\frac{\partial}{\partial y} \left( 1 - (1 - \delta) \hat{n} \right) \frac{\partial \hat{P}}{\partial y} = \frac{F^*}{\sigma^*} (1 - \hat{n}) - \frac{a}{\sigma^*} \hat{n} \hat{C}, \quad (4.2)$$

$$\frac{\partial^2 \hat{C}}{\partial y^2} = E_1^* \hat{n} \hat{C}, \quad (4.3)$$

with

$$\frac{\partial \hat{C}}{\partial y} = -\frac{E_1^* A^* F^*}{a(A^* + F^*)}, \quad \text{at } y = 0, \quad (4.4)$$

$$\frac{\partial \hat{P}}{\partial y} = 0, \quad \hat{C} + \hat{P} = 1, \quad \text{at } y = 0, \quad (4.5)$$

$$\frac{\partial \hat{C}}{\partial y} = 0, \quad \frac{\partial \hat{P}}{\partial y} = 0, \quad \text{at } y = 1. \quad (4.6)$$

We see that this problem is almost identical to the problem for  $n$ ,  $C$  and  $P$  if we set  $a\hat{C} = C$ . The only difference is in the pressure-oxygen tension boundary condition (4.5). In particular, the  $n$  problem and the  $\hat{n}$  problem are identical and so the density of live cells does not change when the proliferation rate is rescaled; the effect is to increase the oxygen tension throughout the tumour mass, and to alter the pressure field.

## 5 Discussion

In this section we explain the results that were highlighted in the previous section, and use the explicit results from §3 to aid us where appropriate. Before proceeding, we summarise the relevant results. We recall that for  $C > C_2^*$ , at equilibrium the total number of live

cells is

$$\mathcal{N} = \int_0^1 n dy = \frac{F^*}{A^* + F^*}, \quad (5.1)$$

and for  $C > C_1^*$ , the total amount of oxygen being consumed is

$$\mathcal{C} = E_1^* \int_0^1 n C dy = \frac{E_1^* A^* F^*}{A^* + F^*}. \quad (5.2)$$

Thus the steady-state total amount of oxygen being consumed per cell is

$$\frac{\mathcal{C}}{\mathcal{N}} = \frac{E_1^* \int_0^1 n C dy}{\int_0^1 n dy} = E_1^* A^*. \quad (5.3)$$

### 5.1 Oxygen consumption rate

To understand the behaviour observed when the oxygen consumption rate is varied we proceed as follows. Consider the steady state profiles for which  $E_1^* = 0.1$  and  $E^* = 10$  and  $C > C_2^*$  throughout the tumour mass (see Figure 5). From §3.2, we know that the total density of live cells  $\mathcal{N}$  does not change as  $E_1^*$  varies (see (5.1)) but that the amount of oxygen being consumed  $\mathcal{C}$  increases with  $E_1^*$  (see (5.2)). Since the total number of cells remains the same, but more oxygen is consumed, the blood vessel must dilate in order to supply the additional oxygen that is required. Increasing the width of the blood vessel leads to an increase in cell proliferation near  $y = 0$ . This, in turn, causes a redistribution of the cells towards the blood vessel.

To understand why the cell speed increases with  $E_1^*$ , we note that the density of dead cells is small close to the blood vessel. Thus most of the motile cells there are alive. Since live cells move with speed  $\delta v_m$ , in order to transport the requisite number of cells away from the proliferating region, as  $E_1^*$  increases, higher values of  $v_m$  are needed.

Using (2.29), we may show that the speed in areas devoid of live cells is given by  $v_m = F^*(1 - y)$ . This explains why the two curves corresponding to  $E_1^* = 10$  and 100 have identical behaviours close to  $y = 1$ .

Finally, we note that, with  $E_1^* = 0.1 \ll 1$ , the oxygen tension is approximately spatially uniform with  $C \sim 0.5 = A^*$ , as predicted in §3.4. We observe from Figure 5c that  $v_m \sim 0$ . Moreover, in the limiting case, if  $v_m = \partial P / \partial y = 0$  in (2.29), we find that  $n$  must be spatially independent. Indeed, for large times,  $n \sim F^* / (A^* + F^*) = 0.5$ , as can be seen in Figure 5a.

### 5.2 Apoptosis rate

To understand the behaviour that is observed when the rate of apoptosis is varied, we focus on the steady state profiles presented in Figure 6 for which  $A^* = 0.25$  and  $A^* = 0.5$ . In both cases, since  $C > C_1^*$  throughout the tumour mass, we know that the total number of live cells decreases as  $A^*$  increases (see (5.1)). In addition, from (5.2), the total amount of oxygen being consumed by the cells also increases. So that these two conditions hold, the supply oxygen tension must increase.

As stated previously, since the density of live cells increases as the apoptosis rate

decreases, the majority of the cell flux must be due to live cells, and so the speed must increase to facilitate this motion.

### 5.3 Degradation rate

To understand the behaviour we observe as the degradation rate  $F^*$  is changed we proceed as follows. From Figure 7 we note that, at equilibrium,  $C > C_2^*$  in all three cases in the steady state (and  $C > C_1^*$  for  $F^* = 0.25, 0.5$ ). Using (5.1), we deduce that the total number of live cells increases with  $F^*$ . From (5.2) we deduce that the total amount of oxygen being consumed also increases with  $F^*$  and thus the supply oxygen tension must increase. Since the supply oxygen tension increases, proliferation near  $y = 0$  increases and, hence, there are more live cells near to the blood vessel. However, since  $\mathcal{C}/\mathcal{N}$  remains constant as  $F^*$  varies (see (5.3)), the oxygen tension away from the blood vessel must decrease as  $F^*$  increases. The cell speed follows the same trends as described before.

### 5.4 Motility

We explain the behaviour that is observed in Figure 8, as the motility coefficient  $\delta$  changes, as follows. Here,  $C > C_2^*$  in all three steady states, and  $C > C_1^*$  for  $\delta = 0.2, 0.5$ . From (5.1), we note that changing  $\delta$  does not affect the total number of live cells  $\mathcal{N}$  in the steady state. However, since decreasing  $\delta$  favours transport of dead cells, the density of live cells close to the blood vessel increases, and the density of live cells away from the blood vessel decreases. Additionally, for small values of  $\delta$  an area consisting completely of dead cells is formed away from the vessel. This is a direct consequence of the rearrangement required by pinning the live cells: it is not caused by necrosis. From (5.2), we can see that the total amount of oxygen being consumed in the steady state is also unchanged as  $\delta$  varies. Since the live cell population at distance from the vessel becomes extinct as  $\delta$  decreases, consumption of oxygen in such a region falls to zero and so the oxygen tension there rises. To satisfy (5.2) and to maintain a constant amount of oxygen being consumed in the steady state, the supply oxygen tension must correspondingly fall. The cell speed follows the same pattern as before: the maximum cell speed increases as the maximum density of live cells (which occurs at the blood vessel) increases, with both maxima increasing with  $\delta$ .

### 5.5 Observations

Guided by the results presented in Figures 5–8, we conclude this section by noting that the system parameters may be grouped into two families  $(E_1^*, F^*)$  and  $(A^*, \delta)$ . As  $E_1^*$  and  $F^*$  increase, the supply oxygen tension and the live cell density close to the vessel increase. By contrast, as  $A^*$  and  $\delta$  increase, the supply oxygen tension increases but the live cell population close to the vessel decreases. Further, changes in  $E_1^*$  and  $F^*$  effect volume changes within the tumour mass (see (2.1), (2.2)), whereas variation of  $A^*$  or  $\delta$  does not.

## 6 Conclusions

We have presented a mathematical model to describe microscale interactions between tumour cells and a compliant blood vessel within a vascular tumour. When developing

the model, we assumed that the tumour mass comprised a mixture of live and dead cells. The live cells proliferated if sufficient levels of oxygen were present in the tissue, and died by apoptosis and oxygen-induced-necrosis (when the level of oxygen in the tissue fell below a critical threshold). The dead cells were removed from the system by enzyme degradation, the enzymes being present in the extracellular matrix. Whilst both live and dead cells were assumed to move within the mass, the live cells were assumed to move less readily due to their strong attachment to the extracellular matrix. We assumed that the tumour cells consumed oxygen, which diffused through the tumour mass from a compliant vessel, whose thickness changed as the pressure exerted on it by the tumour varied.

Analytical and numerical techniques were utilised to illustrate the qualitative behaviour of the model solutions and the system was observed to settle to a steady state (see Figure 4). In the steady state, cell motion was directed away from the blood vessel and the density of live cells and the oxygen tension attained maxima at the blood vessel (see Figures 5–8).

In our model, ‘traditional’ necrosis, that is, cell death (and the formation of a region of dead cells) due to oxygen starvation, is a transient property in all cases except where the oxygen consumption rate is very large. We have demonstrated that an area consisting entirely of dead cells in the middle of the tumour mass can be generated without necrotic death: rather it is due to the live cells moving more slowly than the dead cells. This observational result has implications for the measurement of necrotic oxygen tensions, since, if true, it means that existing estimates of necrotic tensions are too high. We recommend that experiments be carried out to verify whether this is the case. These experiments would involve measuring the oxygen tension in an area of ‘necrosis’ *in vivo*, and then culturing a monolayer of tumour cells, at the same oxygen tension and observing whether they remain viable.

We note that alternative mechanisms for forming areas of dead cells (that is, other than by oxygen-induced-necrosis) already exist in the literature. For example, in Landman & Please [18] and Please *et al.* [25], two pressures are tracked, one in the cells and one in the extracellular component, and areas of ‘necrosis’ are assumed to form when the two pressures become equal. Our model could be modified to examine the effects of this and other necrosis mechanisms.

A weakness of our model concerns the interactions between the tumour cells and the blood vessel: the vessel automatically expands or contracts so that the tumour mass received the requisite amount of oxygen. In particular, we are unable to specify the value of the supply oxygen tension for all time (as we might hope to do for a large, mature vessel with well-developed walls). This is because we are forced to effect a scaling which balances the two sides in (2.8), since this boundary condition is, in this formulation, a condition for  $P$ . If we attempt to take the limit  $k \rightarrow \infty$ , the scaling  $P_0 - P_B = kh_B \rightarrow \infty$ . This issue should be resolved when we recast the problem into higher dimensions.

There are many ways in which our model could be extended and improved and some of these are discussed below. Our model generalises naturally to higher spatial dimensions, the conservation of mass equations being replaced by their three-dimensional counterparts: for example (2.1) would generalise to give

$$n_t + \nabla \cdot (n\mathbf{v}_n) = \lambda n C \mathcal{H}(C - C_1) - An - Nn \mathcal{H}(C_2 - C). \quad (6.1)$$

When solving (6.1), additional boundary conditions must be imposed on the extra domain

boundaries. The most significant change that occurs when the model is reformulated in higher spatial dimensions relates to the equations governing the blood vessel. In particular, full account must be taken of the blood flow along the vessel [20].

As noted in the introduction, other components are present in the tumour tissue apart from tumour cells. In future work we shall include an additional extracellular component which acts as a volume source for the increase in volume that accompanies cell growth and division and a volume sink for the degradation products of dead cells (see Landman & Please [18] for a multiphase model for an avascular tumour and [9] for general two-phase flow models). We shall also relax the assumption that the blood vessels are fixed in space. Thus the size of the microenvironment may vary due to influx of water through the vessel walls. We note that the model presented in this paper may be viewed as a special limit of the more general multiphase model, in which the extracellular water component has constant density throughout the tumour volume.

In our model, simple functional relationships were employed for all the mechanisms included, the aim being to illustrate the qualitative behaviour of the system. Of course, more complex, physically based forms should be used to describe these processes. For example, we could follow Ward & King [28] and modify the apoptosis rate so that it increases with decreasing oxygen tension by setting

$$A(C) = B \left( 1 - \frac{\chi C^m}{C_d^m + C^m} \right). \quad (6.2)$$

Guided by the results presented in Ward & King [28], we believe that the qualitative behaviour of the system would not be altered greatly by such modifications.

Another area of interest concerns the effect of hypoxia on blood vessel collapse and vascular re-modelling [6]. Once a constricted blood vessel falls below a critical size, it supplies no oxygen to the system. The vessel then has only a finite time to re-open, before the endothelial cells that form its walls die and the surrounding tissue becomes anoxic. Under hypoxia, the tumour tissue expresses angiogenic factors (*e.g.* VEGF, TNF- $\alpha$ , TGF- $\beta$ ) which diffuse through the tissue and stimulate the in-growth of new vessels into the hypoxic area. Thus it is clear that the ability of the tumour tissue to become re-perfused depends crucially on the timescales for cell death, diffusion of the angiogenic factors, angiogenesis, and vessel removal. We aim to extend our model to include the production of angiogenic factors and in-growth of new blood vessels in order to determine how the different mechanisms interact to cause re-perfusion of the area.

Our longer term goal is to use the knowledge obtained from studying the microscopic model presented in this paper in the systematic development of a macroscopic model to describe vascular tumour growth. We hope such a model, which will depend heavily on the microscopic parameters, will be invaluable to biologists and clinicians in determining the likely evolution of vascular tumours, given intrinsic properties of the tumour cells in question. The model could easily be adapted to study the effects of different treatment methods (for example, changing the apoptotic potential or changing the rate of cell degradation). Further, the effects of manipulating the endothelial cells that form the blood vessel (*e.g.* changing their rates of apoptosis, or their migration and differentiation characteristics) using agents such as endostatin and angiostatin on the tumour evolution could also be determined [13].

### Acknowledgements

CJWB would like to acknowledge many helpful discussions with Dr D. P. Donovan. This work was carried out with the financial support of an EPSRC Ropa award (CJWB).

### References

- [1] ALBERTS, B., BRAY, D., LEWIS, J., RAFF, M., ROBERTS, K. & WATSON, J. D. (1994) *Molecular Biology of the Cell (3rd Ed)*. Garland Publishing.
- [2] ANDERSON, A. R. A. & CHAPLAIN, M. A. J. (1998) Continuous and discrete mathematical models of tumour-induced angiogenesis. *Bull. Math. Biol.* **60**, 857–899.
- [3] BAISH, J. W., GAZIT, Y., BERK, D. A., NOZUE, M., BAXTER, L. T. & JAIN, J. K. (1996) Role of tumour vascular architecture in nutrient and drug delivery: an invasion percolation-based network model. *Microvasc. Res.* **51**(3), 327–346.
- [4] BAXTER, P. S., WEMYSS-HOLDEN, S. A., DENNISON, A. R. & MADDERN, G. J. (1998) Electrochemically induced hepatic necrosis: the next step forward in patients with unresectable liver tumours? *Aust. Nz. J. Surg.* **68**(9), 637–640.
- [5] BELIEN, J. A. M., VAN DIEST, P. J. & BAAK, J. P. A. (1999) Relationships between vascularization and proliferation in invasive breast cancer. *J. Pathol.* **189**, 309–318.
- [6] BICKNELL, R., LEWIS, C. E. & FERRARA, N. (EDS.) (1997) *Tumour Angiogenesis*. Oxford University Press.
- [7] BYRNE, H. M. & CHAPLAIN, M. A. J. (1995) Growth of nonnecrotic tumours in the presence and absence of inhibitors. *Math. Biosci.* **2**, 151–181.
- [8] BYRNE, H. M. & CHAPLAIN M. A. J. (1995) Mathematical models for tumour angiogenesis: Numerical simulations and nonlinear wave solutions. *Bull. Math. Biol.* **57**(3), 461–486.
- [9] DREW, D. A. (1983) Mathematical modelling of 2-phase flow. *Ann. Rev. Fluid Mech.* **15**, 261–291.
- [10] FOLKMAN, J. (1950) Tumour angiogenesis. *Adv. Cancer. Res.* **43**, 175–203.
- [11] GREENSPAN, H. P. (1976) On the growth and stability of cell cultures and solid tumours. *J. Theor. Biol.* **56**, 229–242.
- [12] GRIFFON-ETIENNE, G., BOUCHER, Y., BREKKEN, C., SUIT H. D. & JAIN R. K. (1999) Taxane-induced apoptosis decompresses blood vessels and lowers interstitial fluid pressure in solid tumours: clinical implications. *Cancer Res.* **59**, 3776–3782.
- [13] HAHNFELDT, P., PANIGRAHY, D., FOLKMAN, J. & HLATKY, L. (1999) Tumour development under angiogenic signalling: a dynamic theory of tumour growth, treatment response and postvascular dormancy. *Cancer Res.* **59**, 4770–4775.
- [14] HELMLINGER, G., YUAN, F., DELLIAN M. & JAIN R. K. (1997) Interstitial pH and pO<sub>2</sub> gradients in solid tumours *in vivo*: High resolution measurements reveal a lack of correlation. *Nat. Med.* **3**(2), 177–182.
- [15] HOCKEL, M., SCHLENGER, K., HOCKEL, S. & VAUPEL, P. (1999) Hypoxic cervical cancers with low apoptotic index are highly aggressive. *Cancer Res.* **59**(18), 4525–4528.
- [16] HOLMGREN, L., O'REILLY, M. S. & FOLKMAN, J. (1995) Dormancy of micrometastases: Balanced proliferation and apoptosis in the presence of angiogenesis. *Nat. Med.* **1**(2), 149–153.
- [17] KROGH, A. (1919) The number and distribution of capillaries in muscles with calculations of the oxygen pressure head necessary for supplying the tissue. *J. Physiol.* **52**, 409–415.
- [18] LANDMAN, K. A. & PLEASE, C. P. (2000) Tumour dynamics and necrosis: surface tension and stability. *IMA. J. Math. Biol.* To appear.
- [19] LEEK, R. D., LEWIS, C. E., GREENALL, M., CLARKE, J. & HARRIS, A. L. (1996) Association of macrophage infiltration with angiogenesis and prognosis in invasive breast carcinoma. *Cancer Res.* **56**(20), 4625–4629.
- [20] LUO, X. Y. & PEDLEY, T. J. (1998) The effects of wall inertia on flow in a two-dimensional collapsible channel. *J. Fluid. Mech.* **363**, 253–280.

- [21] MASEIDE, K. & ROFSTAD, E. K. (2000) Mathematical modelling of chronic hypoxia in tumours considering potential doubling time and hypoxic cell lifetime. *Radiother. Oncol.* **54**, 171–177.
- [22] OCKENDON, J. R., HOWISON, S. D., LACEY, A. A. & MOVCHAN, A. B. (1997) *Applied Partial Differential Equations*. Oxford University Press.
- [23] ORME, M. E. & CHAPLAIN, M. A. J. (1996) A mathematical model of vascular tumour growth and invasion. *Math. Comp. Mod.* **23**(10), 43–60.
- [24] PEDLEY, T. J., BROOK, B. S. & SEYMOUR, R. S. (1996) Blood pressure and flow rate in the giraffe jugular vein. *Phil. Trans. R. Soc. Lond. B* **351**, 855–866.
- [25] PLEASE, C. P., PETTET, G. J. & MCELWAIN, D. L. S. (1999) Avascular tumour dynamics and necrosis. *Math. Mod. Meth. Appl.* **9**(4), 569–579.
- [26] SLEEMAN, B. D. & NIMMO, H. R. (1998) Fluid transport in vascularised tumours and metastasis. *IMA J. Math. Appl. Med.* **15**(1), 53–63.
- [27] VAUPEL, P., KALLINOWSKI, F. & OKUNIEFF, P. (1989) Blood flow, oxygen and nutrient supply and metabolic microenvironment of human tumours: a review. *Cancer Res.* **49**, 6449–6465.
- [28] WARD, J. P. & KING, J. R. (1997) Mathematical modelling of avascular tumour growth. *IMA J. Math. Appl. Med.* **14**, 39–69.
- [29] WEIDNER, N. (1999) Tumour vascularity and proliferation: clear evidence of a close relationship. *J. Pathol.* **189**, 297–299.